Journal of Engineering Mathematics **40:** 91–108, 2001.

A priori evaluation of dynamic subgrid models of turbulence in square duct flow

PETER L. O'SULLIVAN*, SEDAT BIRINGEN and ASMUND HUSER[1]
Department of Aerospace Engineering, University of Colorado at Boulder, Boulder, CO 80309-0429, U.S.A.
e-mail: biringen@spot.colorado.edu
[1]*Safety & Process Advisory Services/DN670, Det Norske Veritas, N-1322 Høvik, Norway*

Received 8 April 1999; accepted in revised form 17 April 2000

Abstract. *A priori* tests of two dynamic subgrid-scale (SGS) turbulence models have been performed using a highly resolved direct numerical simulation database for the case of turbulent incompressible flow in a straight duct of square cross-section. The model testing is applied only to the homogeneous flow direction where grid filtering can be applied without the introduction of commutation errors. The first SGS model is the dynamic (Smagorinsky/eddy viscosity) SGS model (DSM) developed by Germano *et al.* [1] while the second is the dynamic two parameter (mixed) model (DTM) developed by Salvetti and Banerjee [2]. For the Smagorinsky model we have used both the Fourier cut-off filter and a modified Gaussian filter which has the property that it removes aliasing errors in consistent *a priori* model-testing for spectral-based datasets. Results largely consistent with those found for plane channel flow are observed but with some slight differences in the corner regions. As found in prior studies of this sort, there is a very poor correlation of the modelled and exact subgrid-scale dissipation in the case of the DSM. The DSM over-predicts subgrid-scale dissipation on average. Instantaneously, the model provides an inaccurate representation of subgrid-scale dissipation, in general underestimating the magnitude by approximately one order of magnitude. On the other hand, the DTM shows excellent agreement with the exact SGS dissipation over most of the duct cross-section with a correlation coefficient of approximately 0·9.

Key words: square duct, turbulence, subgrid-scale, modelling, numerical simulation

1. Introduction

Turbulent flow in a duct of square cross-section may be considered a generic testbed for the study of complex geometry flows in a similar fashion to the backward-facing step problem, for example. Turbulent flow along sharp corner regions induces a mean secondary flow of the second kind, as classified by Prandtl [3, 4]. The mean motion is towards the corner along the corner bisector and is caused by mean gradients in Reynolds stress. Although the magnitude of the secondary vortical flow is quite weak (around 2–3% of the bulk streamwise velocity) the ramifications for wall shear, heat transfer rates and transport of passive particles is quite significant [5, 6] .

The generation of mean streamwise vorticity in the corner regions has engineering implications for such problems as wing-body junctures with effects on lift to drag ratios etc. Therefore, it is important for any engineering turbulence models to correctly capture the mean secondary motion together with an accurate description of time-dependent flow structures (*e.g.*, for unsteady or non-equilibrium flows). The large-eddy simulation (LES) technique is an evolving computational methodology which (ostensibly) permits accurate phase information

*Current address: Bell Laboratories, Lucent Technologies, Murray Hill, NJ 07974, U.S.A.

for the large scale coherent structures/motions in the flow while providing an effective subgrid-scale (SGS) dissipation term in the model equations. The most widely used SGS model is the eddy viscosity-based model for SGS turbulent stress which posits a linear (tensorial) relationship between SGS stress and the resolved strain rate tensor. Germano *et al.* [1] refined this modelling assumption to compute the Smagorinsky coefficient as a spatially and temporally varying quantity in the flow and hence developed a dynamic approach to SGS modelling.

The dynamic procedure (and its various refinements) has proven extremely effective in LES of canonical flows such as *e.g.*, plane channel flow. It has found some application in complex geometry flows (*e.g.*, the backward-facing step) with satisfactory results [7]. For turbulent flow in square ducts, Madabhushi and Vanka [8] performed an LES using the (constant coefficient) Smagorinsky model with some degree of success. However, near the walls and especially in the corner regions, their LES results did not compare well with experiment. Balaras and Benocci [9] performed LES using the dynamic Smagorinsky model (DSM) in conjunction with wall conditions and again obtained reasonable qualitative results but did not accurately capture the flow behavior (Reynolds stress and RMS velocity) near walls and in the corners.

Salvetti and Banerjee [2] developed a refined, dynamic two parameter mixed SGS model (DTM), following from the work of Zang *et al.* [10] whose mixed model only contained one free parameter. This model combines the good correlation properties of the scale-similar model [11] with the dissipative nature of the eddy viscosity model. Their two parameter mixed model exhibited superior correlations with the exact SGS stress and SGS dissipation. Salvetti *et al.* [2] then went on to perform actual LES for a free-surface flow and verified a significant improvement in agreement by using their DTM compared with the simpler DSM. Horiuti [13] developed a variant of the DTM and also proposed a three parameter model (as yet untested though in either *a priori* or *a posteriori* tests). He studied the merits of several mixed models and the DSM in both plane channel flow and a mixing layer flow and corroborated the findings of Salvetti and Banerjee [2] in *a priori* tests. In actual LES of these two flows, Horiuti then went on to confirm the correctness of the outcome of his *a priori* tests.

The aim of the current work is to assess the likely performance of both the DSM [1] and the DTM [2] subgrid-scale models in large-eddy simulations of streamwise corner flows. This is accomplished by recourse to *a priori* model testing utilizing a database generated in a low Reynolds number direct numerical simulation. For the DSM we have studied both the Fourier cut-off filter and a modified Gaussian filter (to be explained in Section 5) as applied to the periodic streamwise direction; for the DTM we have used the modified Gaussian filter. In a fully general method for complex flows, the SGS filtering has to be done without the existence of homogeneous directions. Hence, the next step would be to implement the present method with an SGS filter applied in all three directions. An approach of this sort is performed in *e.g.* Zang *et al.* [10], Salvetti and Banerjee [2] and Najjar and Tafti [14]. However, filtering in the wall-normal directions introduces second order commutation errors which we avoid in this work (although very recently Vasilyev *et al.* [15] have developed techniques to address this problem).

2. Numerical methods

The problem that we consider is that of turbulent incompressible flow in a straight square duct. The flow geometry and co-ordinate system are shown in Figure 1. The length of each side of the duct is D and the friction velocity is denoted by $u_\tau^2 = \nu\langle\partial u/\partial n\rangle$ where $\langle\partial u/\partial n\rangle$ denotes

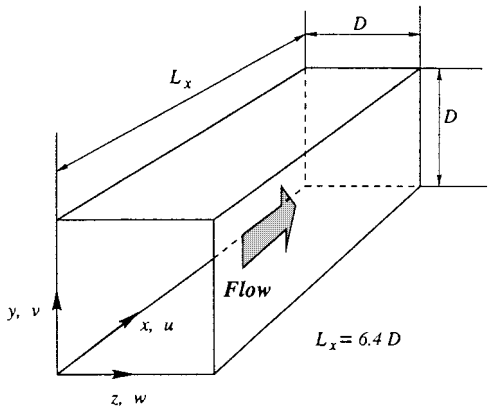

Figure 1. Flow geometry and co-ordinate system.

the mean velocity gradient averaged around the cross-section of the duct and ν is the kinematic viscosity. The friction velocity Reynolds number was taken to be $\mathrm{Re}_\tau = u_\tau D/\nu = 600$ in this study. In closely related previous work [16], and in the present work, the duct length was taken to be $L_x = 6{\cdot}4D$ which was determined to be sufficiently large (based on two point correlation data) to justify the use of periodic boundary conditions in the streamwise direction. The resulting non-dimensional Navier–Stokes equations are

$$\frac{\partial u_i}{\partial t} + \frac{\partial}{\partial x_j} u_i u_j = 4\delta_{i1} - \frac{\partial}{\partial x_i} p + \frac{1}{\mathrm{Re}} \nabla^2 u_i \tag{1}$$

and continuity

$$\frac{\partial u_i}{\partial x_i} = 0.$$

The co-ordinate directions are interchangeably labelled x, y, z or 1, 2, 3 and δ_{ij} is the isotropic tensor. The equations are discretized in space using a Fourier Galerkin procedure in the streamwise (x) direction and fifth order finite differences in the two cross-stream (y and z) directions. The cross-stream (v and w) equations are solved on a staggered mesh which avoids spurious oscillations when the pressure Poisson equation is solved to render the flow divergence-free. The nonlinear products are computed pseudo-spectrally via the 3/2-rule to avoid aliasing errors. Spatial derivatives (in all three directions) are computed using a fifth order upwind-biased method. The flow is advanced in time using the classic operator splitting scheme in conjunction with a third order Runge–Kutta method [17] for the advective terms and Crank-Nicolson for the wall-normal diffusion terms. The related elliptic solvers (for pressure and diffusion) utilize the tensor product method [18]. The numerical grid is stretched in each of the wall-normal directions using an algebraic map which concentrates gridpoints in the corner regions of the duct. Further details of the simulation code may be found in [16] and the references cited therein.

Huser and Biringen [16] previously developed this code and ran it with a spatial resolution of $(N_x, N_y, N_z) = 96 \times 101 \times 101$. With this grid the wall-normal grid spacing is $1{\cdot}8 < \Delta y^+, z^+ < 10$. Their computed results of statistically stationary turbulence at $\mathrm{Re}_\tau = 600$ were in excellent agreement with experimental data. We ran the same direct simulation code for approximately $18D/u_\tau$ time units with somewhat higher streamwise resolution of $N_x = 128$, using as initial conditions a previously archived coarse grid flow field which was almost

fully developed. The coarse grid data were first interpolated onto the current high resolution grid and then after an adjustment phase and complete convergence to statistically stationary turbulent flow we generated an archival database of 80 entire flow realizations spanning a time interval of $11D/u_\tau$. Thus, the individual flow fields are separated in time by an average of $\Delta T = 0{\cdot}1375D/u_\tau$. (The realizations are not uniformly distributed in time as a result of the way we saved some intermediate flow fields.) These instantaneous flow fields are then used to evaluate two SGS turbulence models which are currently in use in large eddy simulations.

3. Filtered equations

The filtering approach to large eddy simulation entails a convolution of the governing equations with a low pass spatial filter which we denote

$$G(\mathbf{x}, \mathbf{y}, \bar{\Delta}) = G\left(\frac{\mathbf{x}-\mathbf{y}}{\bar{\Delta}}\right).$$

In this definition we assume that the filter width, $\bar{\Delta}$, is uniform and that the filter function is translation invariant. This restricts the applicability of the filtering operation to unbounded flow directions. The standard filters are the box, or top hat filter; the cut-off filter which is generally only used in spectral computations and the Gaussian filter. In this work we focus on both the one dimensional Gaussian filter given by

$$G_G(x, \bar{\Delta}) = \frac{1}{\bar{\Delta}}\left(\frac{6}{\pi}\right)^{1/2} \exp(-6x^2/\bar{\Delta}^2)$$

and also the Fourier cut-off filter whose Fourier transform is

$$\bar{G}_{CO}(k, \bar{\Delta}) = \begin{cases} 1 & \text{for} \quad |k| \leq \pi/\bar{\Delta} \\ 0 & \text{for} \quad |k| > \pi/\bar{\Delta} \end{cases}$$

where $k_c = \pi/\bar{\Delta}$ denotes the cut-off wavenumber on the $\bar{\Delta}$ grid. For periodic problems the Fourier transform of the Gaussian filter is given by

$$\bar{G}_G(k, \bar{\Delta}) = \exp(-k^2\bar{\Delta}^2/24)$$

Equation (1) is discretized on a highly resolved spatial grid whose streamwise resolution we denote by δ (with $\delta = L_x/N_x$). We regard the direct numerical solution of these equations on this grid to be an accurate representation of the true fluid velocity field. Upon filtering Equation (1) in the streamwise direction with a filter of characteristic width, $\bar{\Delta}$, we obtain

$$\frac{\partial \bar{u}_i}{\partial t} + \frac{\partial}{\partial x_j}\bar{u}_i\bar{u}_j = 4\delta_{i1} - \frac{\partial}{\partial x_i}\bar{p} + \frac{1}{\mathrm{Re}_\tau}\nabla^2\bar{u}_i - \frac{\partial}{\partial x_j}\tau_{ij} \tag{2}$$

and continuity

$$\frac{\partial \bar{u}_i}{\partial x_i} = 0.$$

Here we define the unresolved subgrid-scale (SGS) stress tensor

$$\tau_{ij} = \overline{u_i u_j} - \bar{u}_i\bar{u}_j - \tfrac{1}{3}(\overline{u_k}u_k - \overline{u}_k u_k)\delta_{ij}$$

(in this last expression for the exact SGS stress we have removed the deviatoric part which is subsumed into the filtered pressure as it would be in an actual large eddy simulation). And, in anticipation of the double- or test-filtering procedure introduced by Germano *et al.* [1, 19] we carry out a second filtering operation with a filter whose width, $\hat{\bar{\Delta}}$, is larger than $\bar{\Delta}$, to obtain

$$\frac{\partial \hat{\bar{u}}_i}{\partial t} + \frac{\partial}{\partial x_j}\hat{\bar{u}}_i\hat{\bar{u}}_j = 4\delta_{i1} - \frac{\partial}{\partial x_i}\hat{\bar{p}} + \frac{1}{\mathrm{Re}_\tau}\nabla^2\hat{\bar{u}}_i - \frac{\partial}{\partial x_j}T_{ij}$$

with

$$T_{ij} = \widehat{\overline{u_i u_j}} - \hat{\bar{u}}_i\hat{\bar{u}}_j - \frac{1}{3}\left(\widehat{\overline{u_k u_k}} - \hat{\bar{u}}_k\hat{\bar{u}}_k\right)\delta_{ij}.$$

In the next two sections we recapitulate the dynamic procedure for modelling the unresolved terms in the large eddy Equations (Equation (2)).

4. Dynamic subgrid-scale models

The dynamic Smagorinsky SGS model (DSM) of Germano *et al.* [1] has proven very successful in LES of turbulence in canonical boundary layer flows such as in a plane channel. This model is based on an eddy viscosity type linear relationship between the SGS Reynolds stress tensor, τ_{ij}, and mean resolved strain rate tensor, $\bar{S}_{ij}$. The model derives from the seminal work of Smagorinsky [20] who applied the model with constant eddy viscosity to atmospheric flow problems. Early applications of the dynamic model generally have been limited to flows with two or three homogeneous directions in which periodic boundary conditions are applied in numerical simulations. This restriction to homogeneous flows circumvents the issue of commutation of spatial differentiation and grid filtering which is a pivotal requirement in high accuracy large eddy simulations. For homogeneous flows (and uniform filter width) the two operations commute whereas for inhomogeneous flows or for non-uniform filter widths this operator commutation breaks down (although recently there have been technical advances in reducing or eliminating the commutation error [21, 15]). In flows with inhomogeneous flow development such as wall bounded turbulence the model has often been applied despite the mathematical inconsistency of grid filtering in wall-normal directions. Nevertheless, attempts have been made (in particular in finite difference calculations) [10, 14, 2] to investigate model performance with the rationale that second order commutation errors may not be any more significant than second order differencing errors which are employed in a great many complex geometry flow solvers.

Thus far the DSM has not been tested *a priori* for the case of turbulent flow in a square duct. Madabhushi and Vanka [8] performed LES for this flow geometry using the (constant coefficient) Smagorinsky model and found only fair agreement with experimental data. Balaras and Benocci [9] subsequently performed LES using the DSM in conjuction with wall boundary conditions and an *ad hoc* clipping procedure to stabilize the computations. Their results indicated a fairly striking similarity between the original Smagorinsky model and the more complex DSM except in the wall regions. Agreement of their computations with experiment was reasonable at best, especially in the wall and corner regions. It is difficult therefore to assess the relative roles played by the three separate SGS numerical procedures in their results.

As a first step in evaluating the DSM for streamwise corner flows we have performed so-called *a priori* tests [22] of the DSM for this flow. In the *a priori* approach to model testing,

data from direct numerical simulation (DNS) can be utilized to make comparisons between the exact SGS Reynolds stresses and the modelled stresses which would reasonably be computed in a large eddy simulation. By reasonable we mean that there is no way of knowing *a priori* what the modelled terms will be since in an LES the grid filtering is implicit in the numerical discretization. However, one can generate plausible synthetic LES flow fields and hence make an educated estimate of the modelled stresses and subgrid-scale dissipation by recourse to consistent model testing as emphasized by Liu *et al.* [23].

4.1. SCALE-SIMILAR MODELS

In a separate approach to SGS turbulence modelling Bardina, Ferziger and Reynolds [11] investigated models of the scale-similarity type. The scale-similar hypothesis posits that the major contribution to SGS stress comes from the interaction of the largest subgrid scales and the smallest resolved scales of motion. Namely, the scales which are 'closest' near the scale cut-off in the model are the ones which contribute most to the SGS energy transfer dynamics. This model was found to improve the correlation with the true subgrid stresses (compared to the correlation coefficient using the Smagorinsky model) in the *a priori* analysis performed by Bardina *et al.* in homogeneous turbulence. In actual LES however, Bardina *et al.* found it necessary to add a Smagorinsky term to provide extra dissipation in order to obtain numerical stability.

The decomposition of the velocity into resolved (filtered) and unresolved parts leads to the following identities

$$u_i = \bar{u}_i + u_i'; \qquad \bar{u}_i = \bar{\bar{u}}_i + \overline{u_i'}. \tag{3}$$

Substituting for u_i in the SGS stress tensor leads to the following decomposition

$$\tau_{ij} = L_{ij} + C_{ij} + R_{ij}$$

where L_{ij}, G_{ij} and R_{ij} are the Leonard, cross and SGS Reynolds stresses, respectively which are given by

$$L_{ij} = \overline{\bar{u}_i \bar{u}_j} - \bar{u}_i \bar{u}_j \qquad C_{ij} = \overline{\bar{u}_i u_j' + u_i' \bar{u}_j} \qquad R_{ij} = \overline{u_i' u_j'}.$$

In general, for two functions f and g it is not true that

$$\overline{fg} = \bar{f}\bar{g}; \tag{4}$$

however, as a closure scheme for LES Bardina *et al.* hypothesized that $\overline{fg}$ might at least be proportional to $\bar{f}\bar{g}$ for turbulent flow data. When this assumption is made for C_{ij} and R_{ij} the following model results

$$C_{ij} = C_B \left[\bar{\bar{u}}_i \overline{u_j'} + \overline{u_i'} \bar{\bar{u}}_j \right] \qquad R_{ij} = C_B \overline{u_i'} u_j',$$

where C_B is a constant. Now, if the second identity of Equation (3) is substituted we find that the sum of C_{ij} and R_{ij} is modeled as

$$C_{ij} + R_{ij} = \beta_{ij} = C_B(\bar{u}_i \bar{u}_j - \bar{\bar{u}}_i \bar{\bar{u}}_j),$$

where β_{ij} is Bardina's scale-similarity model for the unresolved SGS stress.

Speziale [24] has pointed out that C_B must equal unity in order for the Bardina model for τ_{ij} to be Galilean invariant. Recently, Horiuti [13] has argued that the assumption in Bardina's model is not as accurate as the hypothesis that

$$\overline{fg} = \overline{\bar{f}\bar{g}}.$$

Since the filter removes scales below $\bar{\Delta}$ this last expression makes more sense (all scales below the filter width are removed on both sides of the equation). In Bardina's hypothesis, the right hand side of Equation (4) produces scales smaller than the filter width which is at odds with the LHS of the equation, which removes them. However, in an actual LES, there is an additional filtering operation which is not evident in the mathematical analysis. That is, when products are computed numerically there is either an explicit filter in pseudo-spectral codes or an implicit filter for finite difference codes, since the LES grid can not resolve the subgrid scales! This may explain the robustness of the simpler scale-similarity assumption in Equation (4). We note though that Horiuti's variant of the DTM (based on this last hypothesis) involves three filtering operations and is almost 25% more expensive to implement numerically.

4.2. MIXED MODELS

Germano [25] proposed a different way of defining the Leonard, cross and SGS Reynolds stresses which results in each term being separately Galilean invariant (obtained by substituting $\bar{u}_i = \bar{\bar{u}}_i + \overline{u_i'}$ in the second term for τ_{ij}). Hence,

$$\tau_{ij} = L_{ij}^m + C_{ij}^m + R_{ij}^m,$$

where L_{ij}^m, C_{ij}^m and R_{ij}^m are the modified Leonard, modified cross and modified SGS Reynolds stresses, respectively. Explicitly, we have

$$L_{ij}^m = \overline{\bar{u}_i\bar{u}_j} - \bar{\bar{u}}_i\bar{\bar{u}}_j, \quad C_{ij}^m = \overline{\bar{u}_i u_j' + u_i'\bar{u}_j} - \left(\overline{u_i'}\bar{\bar{u}}_j + \bar{\bar{u}}_i\overline{u_j'}\right), \quad R_{ij}^m = \overline{u_i'u_j'} - \overline{u_i'}\,\overline{u_j'}.$$

In the dynamic mixed model of Zang *et al.* [10], L_{ij}^m is computed explicitly and the remaining terms are modelled using the DSM. Salvetti and Banerjee [2] refined this model by introducing a second dynamically computed coefficient for the scale-similar term in the model, yielding the dynamic two parameter model (DTM). In essence, they assume that the modified cross terms are proportional to the modified Leonard stress and once again retain the Smagorinsky model for R_{ij}^m (they note in addition that the second part of R_{ij}^m is negligible). Their DTM has the advantage of providing an extra degree of freedom which can improve the ability of the SGS model to provide 'natural' energy backscatter on the one hand and the correct amount of SGS dissipation on the other. By 'natural' we mean that the energy backscatter is not accounted for necessarily through negative eddy viscosity which is the case in the DSM. This feature of the model greatly reduces the model dependence on the Smagorinsky part of the model and hence also reduces the likelihood of numerical instability in an actual large eddy simulation. More importantly perhaps, the mixed models remove the (false) implicit assumption that the principal axes of the SGS stress tensor be aligned with those of the resolved strain rate tensor.

Finally, we remark that Horiuti [13] has performed a more rigorous analysis than Salvetti and Banerjee [2] where he has developed more sophisticated and rational SGS models for the modified cross and SGS Reynolds stresses, respectively. Unfortunately, these models are more expensive to implement (as mentioned already) and his results indicate only a 5% improvement in correlation coefficients compared with those of the DTM of Ref. [2].

5. Model computation

In performing the dynamic procedure we construct a hierarchy of velocity fields coupled to a hierarchy of spatial grids as follows

u_i = archived DNS flow data at grid-scale δ,

$\bar{u}_i$ = filtered DNS data at grid-scale $\bar{\Delta} = 2\delta$,

$\hat{\bar{u}}_i$ = twice filtered DNS data at grid-scale $\hat{\bar{\Delta}} = 2\bar{\Delta}$.

(We also confine our attention to filter width ratios which are powers of 2). Note that the intermediate grid-scale, $\hat{\Delta}$, satisfies $\hat{\bar{\Delta}}^2 = \hat{\Delta}^2 + \bar{\Delta}^2$ in the case of the Gaussian filter and so $\hat{\Delta} = \sqrt{3}\bar{\Delta}$ in the current investigation. For the spectral cut-off filter we have that $\hat{\Delta} = \hat{\bar{\Delta}}$. We restrict filtering to the x-direction because filtering commutes with spatial differentiation only in this direction for this flow. We emphasize here that in *a priori* tests we have in a sense got all three velocity fields available at the finest grid level, δ. However, when modelling the subgrid and subtest-scale stresses we must compute derivatives based only on information residing at the coarser mesh locations [23], the rationale being that in an actual LES the data would only be available on the $\bar{\Delta}$ grid and not the δ grid. To increase our test sample size we can however compute these coarse mesh derivatives at every fine grid location (using data on the coarser meshes).

5.1. Consistent model testing

In order to perform *a priori* model tests it is necessary to compute terms such as $\bar{S}_{11} = \bar{S}_{xx} = \partial\bar{u}/\partial x$ (such a term occurs in the dynamic computation of the local eddy viscosity). Care must be exercised in this regard so as to avoid incorrectly computing this quantity based on the values of $\bar{u}$ on the DNS grid. Liu *et al.* [23] have emphasized this need to be consistent when performing *a priori* tests using highly resolved flow data. In their work on turbulent jets they computed the spanwise rate of strain element on the $\bar{\Delta}$ grid, $\bar{S}_{33} = \partial\bar{w}/\partial z$ by invoking continuity. The other two components involving z-derivatives, $\bar{S}_{13}$ and $\bar{S}_{23}$, were approximated. We note here that even if one computes such derivatives on this coarser grid (the actual LES grid) there can still be errors depending on the type of grid-filter.

For example, for a periodic problem such as the present duct flow, suppose we have u at $2N$ streamwise gridpoints in physical space. The Fourier transform, $\hat{u}$, therefore has modes in the range $[-(N-1), N]$. If we apply the Gaussian filter to obtain $\bar{u}$ then the SGS frequency content ($|k| \geq N/2$) is non-zero (physical scales in the range $[\delta, \bar{\Delta}]$ remain). To coarsen $\bar{u}$ to the $\bar{\Delta}$ grid, we transform back to physical space and copy/delete every second grid value to form N values for $\bar{u}$. Now, despite the coarsening operation $\bar{u}$ still has SGS information in it, in the form of 'aliasing' error, so to speak. This means that we sample a function which we know has scales in the range $[\delta, \bar{\Delta}]$. Therefore, we need to completely remove all subgrid scales by also cutting off the SGS frequency content ($|k| \geq N/2$ in spectral space). Hence, if we do not completely remove the SGS modes (when using the Gaussian filter) then the velocity field will contain this kind of aliasing error. (This error vanishes however for the case of the sharp cut-off filter in spectral calculations).

Thus, it is important to recognize that under the 'consistent' approach there will possibly be aliasing errors in the resolved strain rate (and, in particular, divergence errors) if the strain rate

is computed without completely filtering out the SGS frequency content. Since the objective of *a priori* tests is to derive synthetic LES flow fields it is important when utilizing DNS data to preserve the divergence-free character of the flow and not to introduce spurious aliasing errors. Hence for the duct DNS data which are spectral-based in x we propose to modify the Gaussian grid- and test-level filters as follows in spectral space

$$\bar{G}_G(k,\bar{\Delta}) = \begin{cases} \mathrm{e}^{-k^2\bar{\Delta}^2/24} & \text{for} \quad |k| \le \pi/\bar{\Delta} \\ 0 & \text{for} \quad |k| > \pi/\bar{\Delta} \end{cases}$$

(and a similar expression for the Fourier transform of the test-level filter). Note that the above filter is in fact the convolution of the cut-off filter (to *completely* remove scales shorter than $\bar{\Delta}$) with the usual Gaussian filter. We emphasize that the use of this filter in no way vitiates the essential ingredients of the dynamic procedure for length scales larger than $\bar{\Delta}$. We also remark that this filter is not strictly positive (with respect to the DNS grid) since the cut-off part in spectral space corresponds to an oscillatory sinc function in physical space.

5.2. Dynamic procedure

Following the approach of Salvetti and Banerjee [2] we adopt the dynamic two-parameter mixed model (DTM) and consider the original DSM of Germano *et al.* [1] as a special case. To avoid confusion we denote the 'exact' subgrid- and subtest-scale stresses by τ_{ij} and T_{ij}. The models which correspond to these terms we denote with a superscript M. That is, we model the 'exact' SGS stress tensor

$$\tau_{ij} = \overline{u_i u_j} - \bar{u}_i\bar{u}_j - \tfrac{1}{3}(\overline{u_k u_k} - \bar{u}_k\bar{u}_k)\delta_{ij}$$

by

$$\tau_{ij}^M = K\left\{\overline{\bar{u}_i\bar{u}_j} - \bar{\bar{u}}_i\bar{\bar{u}}_j - \tfrac{1}{3}(\overline{\bar{u}_k\bar{u}_k} - \bar{\bar{u}}_k\bar{\bar{u}}_k)\delta_{ij}\right\} - 2C\bar{\Delta}^2\|\bar{S}\|\bar{S}_{ij},$$

where $\|\bar{S}\| = (2\bar{S}_{ij}\bar{S}_{ij})^{1/2}$. For the 'exact' sub-test scale terms

$$T_{ij} = \widehat{\overline{u_i u_j}} - \hat{\bar{u}}_i\hat{\bar{u}}_j - \tfrac{1}{3}\left(\widehat{\overline{u_k u_k}} - \hat{\bar{u}}_k\hat{\bar{u}}_k\right)\delta_{ij}$$

we use the same mathematically consistent modelling assumption proposed by Vreman *et al.* [26] (essentially replacing u_i with $\hat{\bar{u}}_i$ underneath all filtering operations) to yield

$$T_{ij}^M = K\{\widehat{\overline{\hat{\bar{u}}_i\hat{\bar{u}}_j}} - \hat{\bar{\bar{u}}}_i\hat{\bar{\bar{u}}}_j - \tfrac{1}{3}\left(\widehat{\overline{\hat{\bar{u}}_k\hat{\bar{u}}_k}} - \hat{\bar{\bar{u}}}_k\hat{\bar{\bar{u}}}_k\right)\delta_{ij}\} - 2\hat{\bar{\Delta}}^2 C\|\hat{\bar{\bar{S}}}\|\hat{\bar{\bar{S}}}_{ij},$$

where $\|\hat{\bar{\bar{S}}}\| = (2\hat{\bar{\bar{S}}}_{ij}\hat{\bar{\bar{S}}}_{ij})^{1/2}$. At this point we employ the Germano identity and a least squares averaging approach in the streamwise direction to evaluate the model 'constants', K and C. For the exact equations we define the 'Germano' tensor

$$L_{ij} = T_{ij} - \hat{\tau}_{ij} = \widehat{\bar{u}_i\bar{u}_j} - \hat{\bar{u}}_i\hat{\bar{u}}_j - \tfrac{1}{3}(\widehat{\bar{u}_k\bar{u}_k} - \hat{\bar{u}}_k\hat{\bar{u}}_k)\delta_{ij},$$

which is a computable quantity in a given large eddy simulation. In order to evaluate the model constants we minimize the mean square error between this tensor and its model

$$L_{ij}^M = T_{ij}^M - \widehat{\tau_{ij}^M} \approx L_{ij}.$$

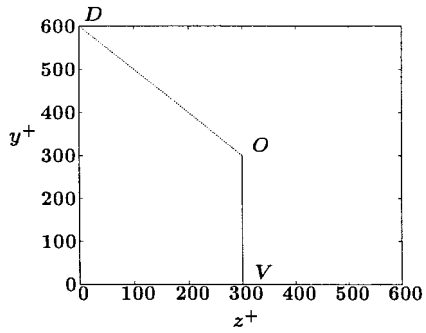

Figure 2. Duct cross-section with wall, OV, and corner bisectors, OD, indicated.

Hence, we find the least-squares solution to

$$T_{ij}^M - \widehat{\tau_{ij}^M} = L_{ij}.$$

If we now let

$$T_{ij}^M - \widehat{\tau_{ij}^M} = K\mathcal{M}_{ij} + C\mathcal{A}_{ij},$$

where

$$\mathcal{M}_{ij} = \left\{\widehat{\bar{\hat{u}}_i\bar{\hat{u}}_j} - \widehat{\bar{u}_i\bar{u}_j}-\right\} + \left\{\widehat{\bar{\bar{u}}_i\bar{\bar{u}}_j} - \hat{\hat{\bar{u}}}_i\hat{\hat{\bar{u}}}_j\right\} - \tfrac{1}{3}\left[\left\{\widehat{\bar{\hat{u}}_k\bar{\hat{u}}_k} - \widehat{\bar{u}_k\bar{u}_k}\right\} + \left\{\widehat{\bar{\bar{u}}_k\bar{\bar{u}}_k} - \hat{\hat{\bar{u}}}_k\hat{\hat{\bar{u}}}_k\right\}\right]\delta_{ij}$$

and

$$\mathcal{A}_{ij} = -2\hat{\bar{\Delta}}^2\|\hat{\bar{S}}\|\hat{\bar{S}}_{ij} + 2\bar{\Delta}^2\widehat{\|\bar{S}\|\bar{S}_{ij}}.$$

then the least squares solution is given by solving the following 2×2 algebraic system (for each y, z, t)

$$\langle\mathcal{M}_{ij}\mathcal{M}_{ij}\rangle K + \langle\mathcal{A}_{ij}\mathcal{M}_{ij}\rangle C = \langle L_{ij}\mathcal{M}_{ij}\rangle \tag{5}$$

$$\langle\mathcal{M}_{ij}\mathcal{A}_{ij}\rangle K + \langle\mathcal{A}_{ij}\mathcal{A}_{ij}\rangle C = \langle L_{ij}\mathcal{A}_{ij}\rangle \tag{6}$$

where $\langle\cdot\rangle$ denotes simple averaging in the homogeneous streamwise direction. Note that the original DSM of Germano *et al.* is recovered simply by setting $K = 0$ and utilizing Equation (6).

6. Results (DSM)

As a first *a priori* test for the current duct flow database we set $K = 0$, i.e., we study the dynamic Smagorinsky SGS model (DSM). In presenting our results we focus mainly on the streamwise-averaged data in the cross-section of the duct together with line plots along both the vertical wall bisector and the upper left corner bisector indicated by the lines OV and OD in Figure 2.

In Figure 3 we illustrate the result of applying both the cut-off filter and the modified Gaussian filter to a single flow realization. The contours of $C(y, z, t)\bar{\Delta}^2$ have been plotted in non-dimensional units of 10^{-5}. From both parts of the figure it is apparent that there is

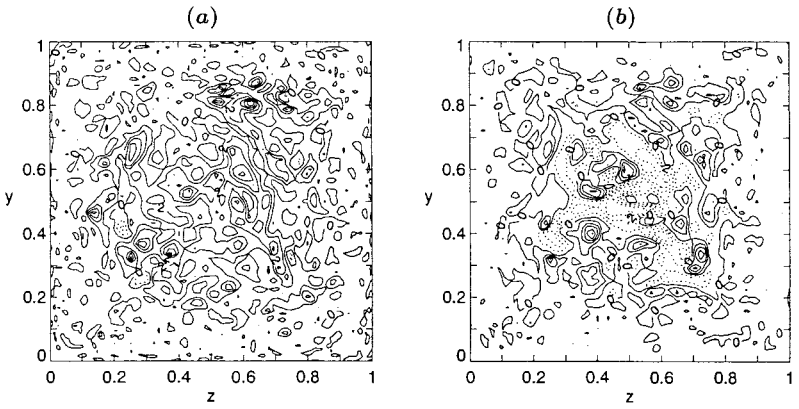

Figure 3. Contours of $C(y, z, t)\bar{\Delta}^2(\times 10^5)$ for the DSM for a single flow realization using (a) the sharp Fourier cut-off filter and (b) the modified Gaussian grid filter. Contour intervals are equally spaced at 2×10^{-5} and negative contours are indicated by a dashed line.

significant backscatter ($C(y, z, t) < 0$) in the central region of the duct for this dataset. The protrusions of non-zero C into the fours corners is also evident illustrating how the near-corner flow has a greater dynamic role in SGS dissipation than the near-wall regions close to the wall bisectors. The asymptotic decay to zero of $C(y, z, t)$ as the duct walls are approached is also clear from each figure. There are differences between parts (a) and (b) of the figure indicating that filter type is having an effect – at least for instantaneous flow realizations. Small scale variations are more evident for the cut-off filter and the near-wall behavior is also different compared with the modified Gaussian filter of part (b) in the figure. The smoother contours in part (b) corresponding to the modified Gaussian filter might have ramifications for an actual LES where spatial derivatives of C can have an important bearing on the numerical stability of the LES. Overall, the use of the cut-off filter results in higher near-wall SGS dissipation compared with the use of the modified Gaussian filter.

In Figure 4a we have plotted a vertical cross-cut of $C(y, z, t)\bar{\Delta}^2$ at the wall bisector, OV, where $z = 1/2$, $z^+ = 300$ for another flow realization. The figure serves to provide more graphical evidence of the comments made in the previous paragraph. In particular, we note the central region of the duct where $C < 0$ for the case of the modified Gaussian filter (dotted curve). We also note that the peaks in C are somewhat larger for the modified Gaussian filter than for the Fourier cut-off filter. In part (b) of the figure we have plotted a diagonal line cut for the same flow realization. The abscissa, d^+, is the diagonal distance, in wall units, from the upper left corner of the duct. The figure indicates that the SGS model is essentially zero for $d^+ < 50$. Over the extended region from $d^+ \approx 50$ to $d^+ = 300$ shown in Figure 4b the Fourier cut-off filter again results in a larger (and positive) C than does the modified Gaussian filter. The modified Gaussian filter also gives a SGS model with a significant proportion of localized backscatter from subgrid to resolved scales (although this in turn depends on the local magnitude of $\|\bar{S}\|$).

6.1. SGS DISSIPATION

The primary role of any eddy viscosity SGS model is to provide dissipation of turbulent kinetic energy via enhanced turbulent viscosity. The SGS 'dissipation' term in the LES equations is given by

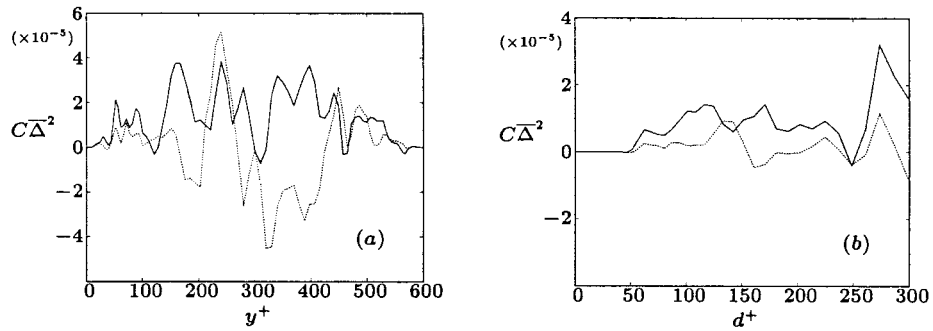

Figure 4. Variation of $C(y, z, t)\bar{\Delta}^2$ along (a) the vertical wall bi-sector $z = 1/2$, $z^+ = 300$ and (b) along the upper left corner bisector. Results are for a single flow realization. Solid curve is for the sharp Fourier cut-off filter and the dotted curve is for the modified Gaussian filter.

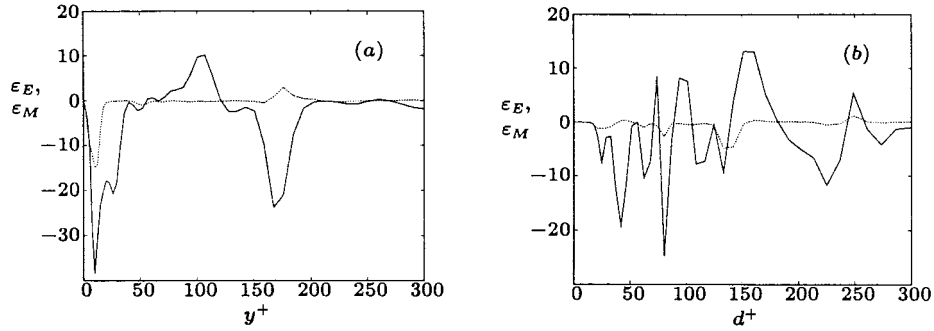

Figure 5. Variation of 'exact' (solid curves) and modelled (dotted curves) SGS dissipation (ε_E and ε_M) at $x = 0$ for a single flow realization: (*a*), along the wall bisector, $z = 1/2$, $z^+ = 300$; and (b), outward along the upper left corner bisector. This data is for the same flow realization as in Figure 4. The DNS data have been filtered using the modified Gaussian filter.

$$\varepsilon = \tau_{ij}\bar{S}_{ij}.$$

This quantity acts as either a source or sink depending on whether $C(y, z, t)$ is negative or positive, respectively. We distinguish between the 'exact' SGS dissipation, ε_E, *i.e.*, that predicted by the filtered DNS data, and the modelled SGS dissipation, ε_M, that is given by

$$\varepsilon_M(x, y, z, t) = -2C(y, z, t)\bar{\Delta}^2\|\bar{S}\|\bar{S}_{ij}\bar{S}_{ij} = -C(y, z, t)\bar{\Delta}^2\|\bar{S}\|^3$$

In Figure 5 we have plotted the variation of both ε_E and ε_M for the same single flow realization that was used for Figure 4 and at a single x-station (the figure depicts data which have been filtered using the modified Gaussian filter). Part (*a*) shows the variation along the vertical wall bisector, OV, while part (*b*) shows the variation along the upper left corner bisector, OD.

The figure demonstrates clearly that in an instantaneous and spatially localized sense there is at best a very poor correlation between the exact and the modelled SGS dissipation. In part (*a*) we can see that there is some good agreement of ε_E and ε_M only in the region $y^+ < 10$ or so. We notice also that the magnitude of the modelled SGS dissipation does not compare favorably with the typical magnitude of the exact quantity. In part (*b*) we see that the model is providing essentially no SGS dissipation in the corner region, $d^+ < 50$. Although these figures are for a single station and a single instantaneous realization they are representative of the model performance in general.

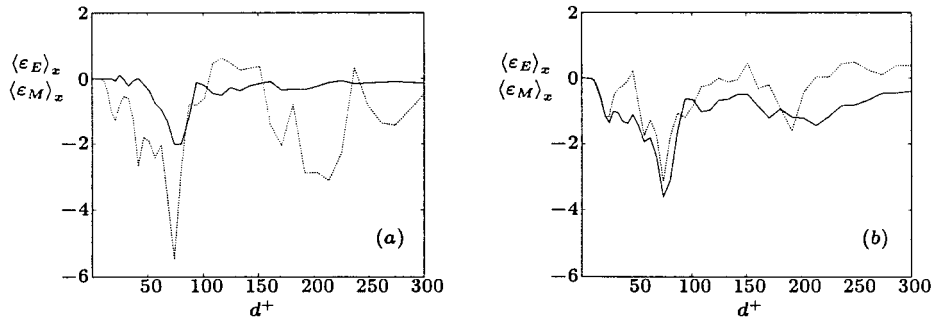

Figure 6. Variation of exact (solid curves) and modelled (dotted curves) streamwise-averaged SGS dissipation ($\langle \varepsilon_E \rangle_x$ and $\langle \varepsilon_M \rangle_x$) for a single flow realization versus distance along the corner bisector. (*a*), using the Fourier cut-off filter and (*b*), using the modified Gaussian filter for a single flow realization.

We comment here that this result indicates, or predicts, very poor phase representation in an actual LES using the DSM: the SGS model might produce sufficiently accurate integrated results such as mean skin friction and Reynolds stress but the LES flow dynamics will most likely be entirely disparate from the true flow evolution since the SGS dissipation term in the governing equations is so inaccurate.

6.2. Spatial mean SGS dissipation

In Figure 6 we have plotted the streamwise-averaged SGS dissipation for the two filter types for another flow realization. Also shown for reference is the exact SGS dissipation in each case. We can see a significant improvement in agreement between the exact and the modelled SGS dissipation although there are still some clear differences. We note that the modified Gaussian filter shown in part (*b*) appears to yield better agreement (in this case). In contrast to the instantaneous behavior of ε_M in relation to ε_E we can see in Figure 6a that the Fourier cut-off filter is predicting an excess in SGS dissipation. For the instantaneous data shown in Figure 5, ε_M was smaller in magnitude than ε_E. This trend is in accord with the underlying principle of the DSM: to provide a statistical balance between production and dissipation. We also note that for both filter types there is a net average (average in x) backscatter ($\langle \varepsilon_M \rangle_x > 0$) at several spatial locations along OD despite the fact that the exact value $\langle \varepsilon_E \rangle_x$ is almost strictly negative for this particular realization.

6.3. Ensemble-average SGS dissipation

In Figure 7 we have plotted the ensemble-averaged exact and modelled SGS dissipation, $\langle \varepsilon_E \rangle$ and $\langle \varepsilon_M \rangle$, where the average is computed over $N_x = 128$ streamwise stations, eight similar octants and eighty flow realizations. We see from both parts of this figure that the filter type is not inconsequential. Both the exact and modelled SGS dissipation are strongly influenced by the specific filter chosen. Along the wall bisector (Figure 7a) we can see that both filters yield approximately the same result for modelled SGS dissipation despite the fact that they each yield quite different results for the exact SGS dissipation. However, in the corner region (Figure 7b) we see that the results for $\langle \varepsilon_M \rangle$ depend on the choice of grid filter. For either filter there is roughly a factor of 2 disparity between $\langle \varepsilon_E \rangle$ and $\langle \varepsilon_M \rangle$ along both the wall and corner bisectors. It is also interesting that along the corner bisector we find that the Fourier cut-off filter yields $\langle \varepsilon_M \rangle < \langle \varepsilon_E \rangle$ whereas the modified Gaussian filter yields $\langle \varepsilon_M \rangle > \langle \varepsilon_E \rangle$.

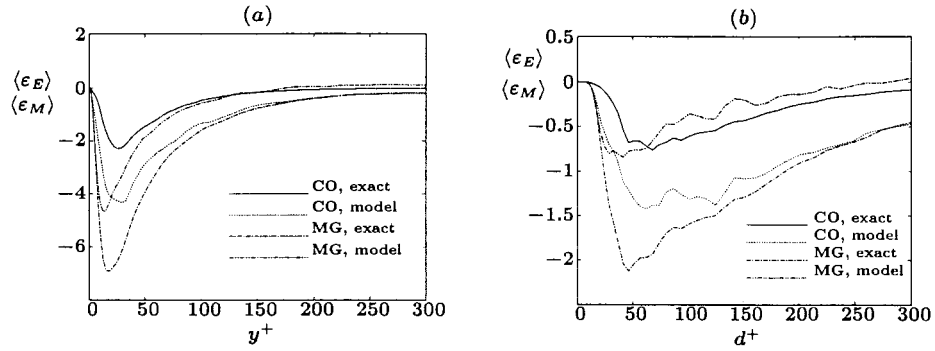

Figure 7. Ensemble-averaged SGS dissipation for both the Fourier cut-off filter and the modified Gaussian filter along (*a*) the wall bisector and (*b*) along the corner bisector. Both the exact and modelled SGS dissipation is plotted for each filter type. In the legend the Fourier cut-off filter and the modified Gaussian filter are denoted CO and MG, respectively.

That is, the Fourier cut-off filter overpredicts SGS dissipation while the modified Gaussian filter underpredicts it in the corner region of the flow. As yet, we do not have an explanation for this dependence on the filter type.

6.4. Correlation coefficient

The overall success of a SGS model is often characterized in terms of the correlation coefficient of the modelled dissipation with the true, exact SGS dissipation (modulo the explicit grid filter). Thus we define

$$\rho(\varepsilon) = \frac{\langle (\varepsilon_M - \langle \varepsilon_M \rangle)(\varepsilon_E - \langle \varepsilon_E \rangle) \rangle}{\langle (\varepsilon_M - \langle \varepsilon_M \rangle)^2 \rangle^{1/2} \langle (\varepsilon_E - \langle \varepsilon_E \rangle)^2 \rangle^{1/2}}.$$

In Figure 8 we have plotted the spatial variation of $\rho(\varepsilon)$ along OV and OD for both the Fourier cut-off filter and the modified Gaussian filter. From this figure we see very clearly that the correlation for the DSM is very poor regardless of filter type with $\rho(\varepsilon)$ in the range 0–0·2. The modified Gaussian filter correlates somewhat better especially in the regions y^+, $d^+ < 100$ or so but is still on a par with the results found previously in similar studies of plane channel turbulence. In light of this result, we conclude that for spectral-based simulations the modified Gaussian filter is the superior filter especially in the region y^+, $d^+ < 150$.

7. Results (DTM)

In this section we present results for computations performed using the complete DTM ($K \neq 0$). We used the modified Gaussian filter for these tests and note here that the scale-similar part of the SGS model is identically zero if one uses the Fourier cut-off filter. In this case, $\bar{u}_i = \bar{\bar{u}}_i$ and hence, numerically, in a pseudo-spectral LES $\overline{\bar{u}_i \bar{u}_j} = \bar{\bar{u}}_i \bar{\bar{u}}_j$. The RHS of this last expression generates Fourier modes above the spectral cut-off, but they are cut-off implicitly by the finite numerical discretization itself.

An example of the Smagorinsky coefficient, C, computed using the DTM is shown in Figure 9 together with the corresponding C computed via the DSM (modified Gaussian filter). The order of magnitude is the same in each case but, significantly, for the DTM we see that $C > 0$ almost throughout the entire domain. We have found this to be true in nearly all other

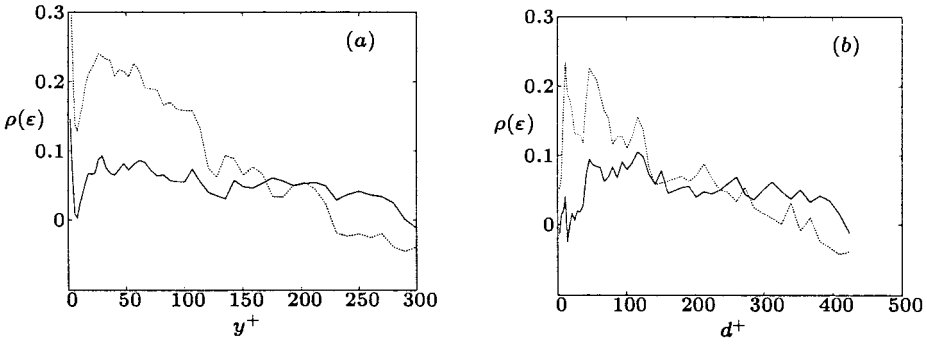

Figure 8. Correlation coefficient for SGS dissipation along (*a*) the wall bisector and (*b*) the corner bisector. Solid curves denote results based on the Fourier cut-off filter and dotted curves denote results based on the modified Gaussian filter.

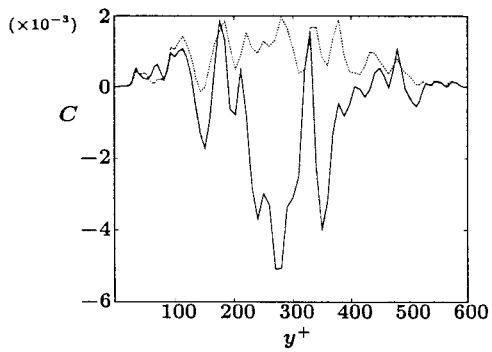

Figure 9. Smagorinsky coefficient, C, for a single flow realization *versus* distance along the wall bisector. Solid curve: DSM (modified Gaussian filter) and dotted curve: DTM.

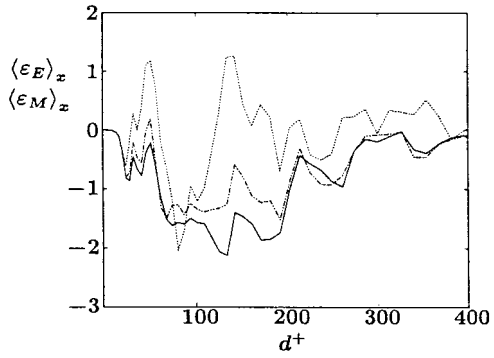

Figure 10. Streamwise-averaged SGS dissipation, $\epsilon\langle(x, y, z, t)\rangle_x$, for a single flow realization *versus* distance along the corner bisector. Solid curve: exact; dotted curve: DSM (modified Gaussian filter) and chain-dashed curve: DTM.

realizations. The fairly rapid fluctuations in C with the DSM are removed with the DTM. Thus, in an actual LES the DTM will most likely produce a more stable (numerically) SGS model. Firstly, the absence of large negative C will produce a positive total viscosity. Secondly, the reduction in slope ($\partial C/\partial y$ etc.) will also help to stabilize numerical implementation.

The second parameter, K, in the DTM obtains an average value of approximately 1·75 in the cross-section of the duct with slightly higher values near the walls and corners ($K \approx 2{\cdot}0 - 2{\cdot}5$). This is consistent with Horiuti's value ($K \approx 1{\cdot}75$) for *a priori* tests of plane channel flow at $\mathrm{Re}_\tau = 180$ [13]. Salvetti and Banerjee [2] obtained $K = 1{\cdot}3$ in *a priori* tests of free-surface plane channel turbulence at $\mathrm{Re}_\tau = 171$ (based on the total channel depth). Hence, their Re_τ is 85·5 in the more common scaling based on channel half-height. In actual LES, Salvetti *et al.* [12] studied the same problem with the same Re_τ but with decaying turbulence and obtained $K \approx 1{\cdot}2$ throughout the channel depth. The difference is most likely a result of different Re_τ. We note that departures of K from unity indicate the relative contribution of the modified cross terms compared with the modified Leonard tensor but that the scale-similarity hypothesis is still being used (to model the cross terms).

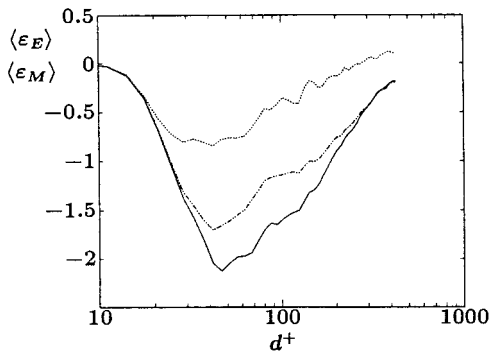

Figure 11. Ensemble-averaged SGS dissipation versus distance along the corner bisector. Solid curve: exact; dotted curve: DSM (modified Gaussian filter) and chain-dashed curve: DTM.

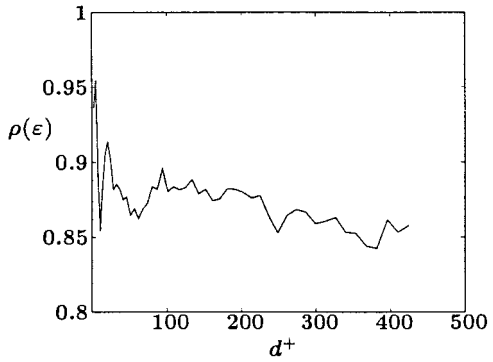

Figure 12. Correlation coefficient for SGS dissipation along the corner bisector for the DTM.

In Figure 10 we have plotted the streamwise-averaged exact and modelled SGS dissipation for a single flow realization. For comparison we have also plotted ε_M based on the DSM with modified Gaussian filter. The abscissa is the diagonal distance along DO measured in wall units. We see that the DTM result comes into close agreement with the exact data almost throughout the entire region. In contrast, the result from the DSM is markedly in error. The DSM predicts a large region of backscatter (in $40 < d^+ < 60$ and $120 < d^+ < 185$) whereas the DTM captures the (correct) forward scatter which characterizes this region at this instant. Both in the region $0 \leq d^+ < 60$ and also $d^+ > 200$ the DTM is in excellent agreement with the exact data. In the remaining region $60 < d^+ < 200$ the model's performance is not quite as good but it is still dramatically superior to the DSM.

7.1. Ensemble-average SGS dissipation

The corresponding ensemble-averaged SGS dissipation is shown in Figure 11 where, again, we have included the DSM result for comparison. The DTM exhibits a significant improvement over the DSM (with modified Gaussian filter). The logarithmic scaling of the abscissa highlights the remaining region where the DTM is not in excellent agreement with the exact data ($30 < d^+ < 200$ or so). However, even here the DTM predicts the SGS dissipation to within 30% (at worst) while the DSM is at best within in 75% of the exact data. In the outer region of the flow the DTM show an even more striking agreement with the exact data while the DSM is in error both quantitatively and qualitatively (incorrectly predicting backscatter (on average) from $280 < d^+ < 424{\cdot}26$).

The corresponding correlation coefficient (along DO) is plotted in Figure 12. The almost uniform value of $\rho(\varepsilon) \approx 0{\cdot}875$ for the DTM should be compared with the value $\rho(\varepsilon) < 0{\cdot}2$ for the DSM. This result together with improved agreement in instantaneous flow realizations (for SGS dissipation) strongly suggests that the DTM will yield a very good SGS modelization for flows in the square duct geometry. The removal of incorrectly predicted regions of backscatter (compared with DSM) should also mitigate numerical instability problems in an actual LES for these types of flow.

8. Conclusions

We have analyzed a large computational database for incompressible duct flow at $\mathrm{Re}_\tau = 600$ in order to assess the probable performance of both an eddy viscosity and a mixed type dynamic SGS turbulence model in a LES. We have clarified a technical point regarding the consistent *a priori* test approach [23] for spectral-based data and we arrived at a modified Gaussian grid filter which removes aliasing errors when derivatives are computed on the (synthetic) LES grid. This property is important in preserving the divergence-free character of the synthetic LES flow fields that are generated in a consistent model testing approach.

In accord with prior studies on channel turbulence we have found in these *a priori* tests that the DSM correlates very poorly with the exact SGS stress (as inferred from the correlation of SGS dissipation). We also found that the filter type did have an effect on the model performance, notwithstanding the poor correlation in either case. The DSM performance in the corner regions of the duct was essentially the same as in the wall region near the wall bisector with a correlation coefficient (for SGS dissipation) of at best 0·2.

We also tested the dynamic two parameter model (DTM) proposed by Salvetti and Banerjee [2] and found that it provides excellent agreement over most of the duct cross-section. The correlation coefficient of SGS dissipation was approximately 0·9 for most of the duct. Instantaneous flow realizations also indicate that the DTM is quite successful in capturing the instantaneous SGS energy transfer dynamics near the walls, corners and in the outer flow. However, the performance is somewhat diminished in the outer log regions. The Smagorinsky coefficient in the DTM is generally positive indicating that that part of the model is capturing forward scatter while the majority of the backscatter is being modelled by the scale-similar part. In general, false predictions of backscatter in the DSM are removed with the use of the DTM. The Smagorinsky coefficient of the DTM is also smoother than that of the DSM which will have ramifications in an actual LES. These two properties of the DTM suggest that it will perform well in an actual LES, primarily due to the superior physical model predictions but also because of the superior numerical stability properties which follow from a smoother positive Smagorinsky coefficient. Recent *a posteriori* tests of two parameter mixed models have in fact borne this out for a number of flows [12, 13].

The DTM has shown to be promising towards development of robust, accurate and physically correct LES. To make the model more general, further work needs to be done. First, there is the need to devise an accurate (4th order or better) method for filtering in inhomogeneous directions. Second, focus must also be on high Re and the associated required wall resolution. Only when these two issues are resolved can LES be applied for industrial flows as a predictive tool.

Acknowledgements

The authors wish to thank Dr. L. Patrick Purtell for his continued interest in this research. Also, the comments of the referees served to improve upon an earlier draft of this paper. This research has been funded in part by the National Science Foundation under grant ECS-9725504 and also by the Office of Naval Research under grant DOD N00014-95-1-0419. Computations were performed on a Cray C916 at the US Army Corps of Engineers, Waterways Experiment Station, Vicksburg, MS. The authors thank Professor Steve Orszag for his very helpful comments during the initial phase of this research.

References

1. M. Germano, U. Piomelli, P. Moin, and W. H. Cabot, A dynamic subgrid-scale eddy viscosity model. *Phys. Fluids A* 3 (1991) 1760–1765.
2. M. V. Salvetti and S. Banerjee, *A priori* tests of a new dynamic subgrid-scale model for finite-difference large-eddy simulations. *Phys. Fluids* 7 (1995) 2831–2847.
3. L. Prandtl, Über die ausgebildete Turbulenz. In: *Verh. 2nd Intl. Kong. für Tech. .Mech., Zürich* (1926) 62–83. [Eng. transl. NACA Tech. Memo. 435].
4. L. Prandtl, *Essentials of Fluid Dynamics*. London: Blackie (1967) 152 p.
5. A. O. Demuren and W. Rodi, Calculation of turbulence-driven secondary motion in non-circular ducts. *J. Fluid Mech.* 140 (1984) 189–222.
6. A. O. Demuren, Calculation of turbulence-driven secondary motion in ducts with arbitrary cross-section. *AIAA J.* 29 (1991) 531–541.
7. K. Akselvoll and P. Moin, Application of the dynamic localization model to large-eddy simulation of turbulent flow over a backward facing step. In: U. Piomelli and S. Ragab (eds.): *Engng. Applic. Large Eddy Simul.* 162 (1993) 1–12.
8. R. K. Madabhushi and S. P. Vanka, Large eddy simulation of turbulence-driven secondary flow in a square duct. *Phys. Fluids A* 3 (1991) 2734–2745.
9. E. Balaras and C. Benocci, Large eddy simulation of flow in a square duct. In: *Thirteenth Symp. Turbulence*, Rolla, Missouri, (1992) A33–1.
10. Y. Zang, R. L. Street, and J. R. Koseff, A dynamic mixed subgrid-scale model and its application to turbulent recirculating flows. *Phys. Fluids A* 5 (1993) 3186–3196.
11. J. Bardina, J. H. Ferziger, and W. C. Reynolds, Improved turbulence models based on LES of homogeneous incompressible turbulent flow. Report TF-19, Stanford University. Dept. of Mechanical Engineering (1983).
12. M. V. Salvetti, Y. Zang, R. L. Street, and S. Banerjee, Large-eddy simulation of free-surface decaying turbulence with dynamic subgrid-scale models. *Phys. Fluids* 9 (1997) 2405–2419.
13. K. Horiuti, A new dynamic two-parameter mixed model for large-eddy simulation. *Phys. Fluids* 9 (1997) 3443–3464.
14. F. M. Najjar and D. K. Tafti, Study of discrete test filters and finite difference approximations for the dynamic subgrid-scale stress model. *Phys. Fluids* 8 (1995) 1076–1088.
15. O. V. Vasilyev, T. S. Lund, and P. Moin, A General Class of Commutative Filters for LES in Complex Geometries. *J. Comp. Phys.* 146 (1998) 82–104.
16. A. Huser and S. Biringen, Direct numerical simulation of turbulent flow in a square duct. *J. Fluid Mech.* 257 (1993) 65–95.
17. H. Le and P. Moin, An improvement of fractional-step methods for the incompressible Navier-Stokes equations. *J. Comp. Phys.* 92 (1991) 369–383.
18. A. Huser and S. Biringen, Calculation of shear-driven cavity flows at high Reynolds numbers. *Int. J. Num. Meth. Fluids* 14 (1992) 1087–2001.
19. M. Germano, Turbulence: the filtering approach. *J. Fluid Mech.* 238 (1992) 325–336.
20. J. Smagorinsky, General circulation experiments with the primitive equations. I. The basic experiment. *Mon. Weath. Rev.* 91 (1963) 99–164.
21. H. van der Ven, A family of large eddy simulation (LES) filters with nonuniform filter widths. *Phys. Fluids* 7 (1995)) 1171–1182.
22. R. A. Clark, J. H. Ferziger, and W. C. Reynolds, Evaluation of subgrid models using an accurately simulated turbulent flow. *J. Fluid Mech.* 91 (1979) 1–16.
23. S. Liu, C. Meneveau, and J. Katz, On the properties of similarity subgrid-scale models as deduced from measurements in a turbulent jet. *J. Fluid Mech.* 275 (1994) 83–119.
24. C. G. Speziale, Galilean invariance of subgrid-scale stress in large eddy simulation. *J. Fluid Mech.* 156 (1985) 55–65.
25. M. Germano, A proposal for the re-definition of the turbulent stresses in the filtered Navier-Stokes equations. *Phys. Fluids* 29 (1986) 2323–2329.
26. B. Vreman, B. Geurts and H. Kuerten, On the formulation of the dynamic mixed subgrid-scale model. *Phys. Fluids* 6 (1994) 4057–4059.